ISET Journal of Earthquake Technology, ***Technical Note****, Vol. 40, No.1, March 2003, pp. 77-97*

ATHENS EARTHQUAKE OF 7 SEPTEMBER 1999: INTENSITY MEASURES AND OBSERVED DAMAGES

A. Elenas

Department of Civil Engineering
Institute of Structural Mechanics and Earthquake Engineering
Democritus University of Thrace
GR-67100 Xanthi, Greece

ABSTRACT

This paper presents an acceleration parameter study of the 1999 Athens earthquake, and it discusses the capabilities of various acceleration parameters to describe the seismic damage potential. In addition, the destructive consequences of the earthquake are exemplarily displayed by several structural failures. The analysis results have shown that the seismic parameters of the Athens earthquake exhibit a great dispersion in the results. Both low and high numerical values have been observed for all the examined engineering parameters, due to different geological conditions. The structural failures may be attributed first to the proximity of the epicentre to the urban area, and in several cases, to the high vulnerability of the structures due to poor structural detailing and inappropriate construction.

KEYWORDS: Seismic Parameters, Damage Potential, Structural Damage

INTRODUCTION

On September 7, 1999 at 14:56 local time (11:56 GMT), a strong and unexpected earthquake with moderate to strong magnitude, $M = 5.9$, occurred at a small epicentral distance (18 km) from the historical centre of the city of Athens in Greece (Tselentis and Zahradnik, 2000; Papadopoulos et al., 2000; Lekkas, 2001).

At the time of the earthquake, many people were at work, which was the reason that in three collapsed factory facilities, many people died. Fortunately, no injured people were reported at school sites, because the earthquake struck during the summer holidays. An enormous traffic jam made it impossible, almost any movement in the city centre to take place half an hour after the event. The first response and the relief effort immediately after the earthquake focussed on search and rescue operations in the collapsed buildings. The operations were done mainly by the special rescue teams and the firefighting service. Backup support came from the police services and the Army. The restoration of the electricity and the communication facilities began immediately after the event. In addition, an information response system was established for the coordination of the actions dealing with the disaster results.

The day following the earthquake, the Ministry of Environment, Urban Planning and Public Works organised many two-person teams of engineers, which began surveying the affected areas for a rapid damage assessment. The number of buildings classified as “red”, “yellow” and “green” after official inspections in the broader area of Athens, were about 13000, 62000 and 110000, respectively. “Red” indicates buildings damaged beyond repair or heavily damaged but repairable; the buildings should not be used until they are repaired. “Yellow” indicates repairable, minor damage to structural elements, and significant damage to nonstructural elements; the buildings should not be used temporarily, and require repairs before reoccupation. “Green” means no visible damage affecting the structural capacity of the buildings; the buildings can be occupied. About 40 buildings collapsed, causing 143 casualties. In addition, 800 people were injured. The most serious damages were observed at the northern suburbs, which are closer to the epicentral area. During the first days after the earthquake, about 100000 people were rendered homeless. About 16000 tents, 4000 beds, and 8000 blankets were distributed. For the people with damaged houses, immediate financial support was arranged. About 3 billion US Dollars were roughly estimated for the caused tangible loss. From the point of view of economic loss, it is the worst natural disaster reported in the modern history of Greece.

This study presents several seismic acceleration parameters of the Athens earthquake main shock, along with a statistical analysis of them. Additionally, diverse structural failures are exposed to manifest their seismic damage potential.

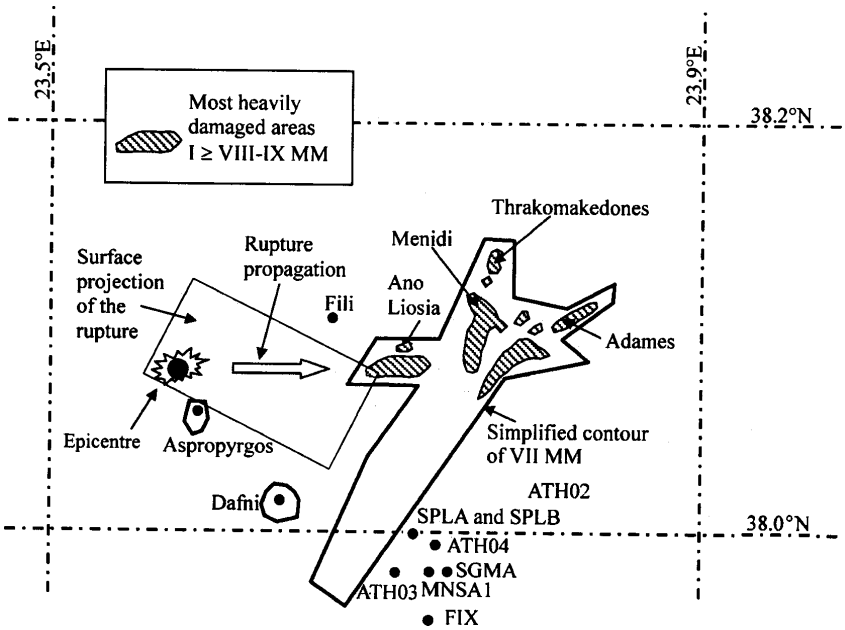

Fig. 1 Regional overview of the epicentre, meizoseismal area, isoseismal lines, and distribution of the accelerographs

STRONG GROUND MOTION AND SEISMIC PARAMETERS

The Institute of Geodynamics of the National Observatory of Athens (Kalogeras and Stavrakakis, 1999) and the Institute of Engineering Seismology and Earthquake Engineering (ITSAK) of Thessaloniki (Anastasiadis et al., 1999) recorded the strong motion from the main shock of the Athens earthquake by eighteen accelerographs. Fourteen were within the central area of Athens. Unfortunately, none of the accelerographs were placed in the most damage-affected areas. Four accelerographs were at the centres of nearby towns of Aliveri, Rafina, Lavrio, and Thiva. Table 1 shows the statistical data of all the horizontal components of the eighteen main shock records. As statistical data, the average, the standard deviation, the minimum and maximum values, and the lower and the upper limits of the 95% confidence interval have been considered (Spiegel, 1992). The records in the present study have been selected by using the criterion that the mean PGA value of the horizontal main shock component is at least equal to 0.1g. Figure 1 presents an overview map with the epicentre of the event, the meizoseismal region, the affected urban area, the intensity distribution, and the positions of the accelerographs (Lekkas, 2001; Decanini et al., 2002). Table 2 presents the event data of sixteen recorded accelerograms. These records fulfil the previously mentioned criterion.

The acceleration record of Monastiraki, near the city centre, provided an isolated peak value of 0.511g (Tables 2 and 4), although no considerable damages were observed in this region. This was probably affected by the complicated foundation conditions and the response of a steel structure covering an archaeological excavation close to the accelerometer. As mentioned previously, no recordings were available at shorter epicentral distances, other than those given in Table 2, for direct assessment of the strong motion characteristics in the epicentral zone and in the most damage-affected areas (Figure 1). Nevertheless, an indirect estimation, based on observed movements (sliding and overturning) at cemeteries close to the epicentral area, suggests that the horizontal PGA may have exceeded 0.5g (Psycharis et al., 1999). Amplification analyses estimated a PGA value as high as 0.6g to 0.7g on stiff soil and soft rock, at a distance of 5 km from the fault (Bouckovalas and Kouretzis, 2001). In addition, Gazetas estimated even higher PGA values on silty-gravel sands and sandy-gravel clays in Adames, at a distance of 9 km from the fault (Gazetas et al., 2002). Bouckovalas et al. (2002) provided average values of PGA for rock and soil conditions, for different distances from the fault rupture. In their work, the estimated PGA values at epicentral areas (1 to 3 km away from the fault) are 0.35g-0.42g for rock sites

and 0.49g-0.57g for soil sites (Bouckovalas et al., 2002). These values may have been locally exceeded, even by 70%, due to data scatters. Based on the data presented, Table 3 shows the estimated mean PGA and the mean distance of the twelve worst affected municipalities, during the Athens earthquake, from the seismic epicentre.

Table 1: PGA Statistical Data of the Main Shock Acceleration Records from the Athens Earthquake

Seismic Parameter	Average	Standard Deviation	Minimum Value	Maximum Value	95% Confidence Interval for Mean	
					Lower Limit	Upper Limit
PGA (g)	0.158	0.107	0.044	0.511	0.117	0.199

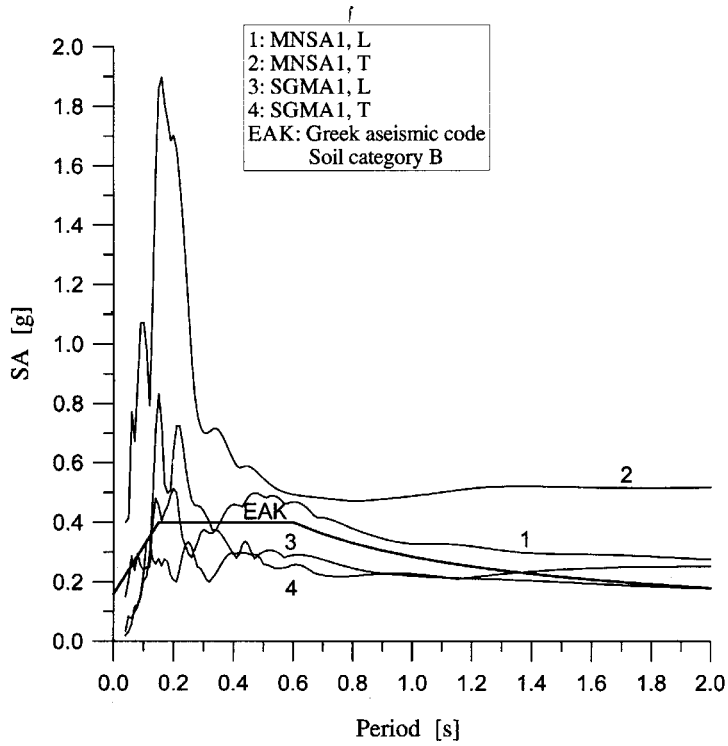

Fig. 2 Elastic response spectra of the accelerograms 1-4 and the recent EAK design spectrum

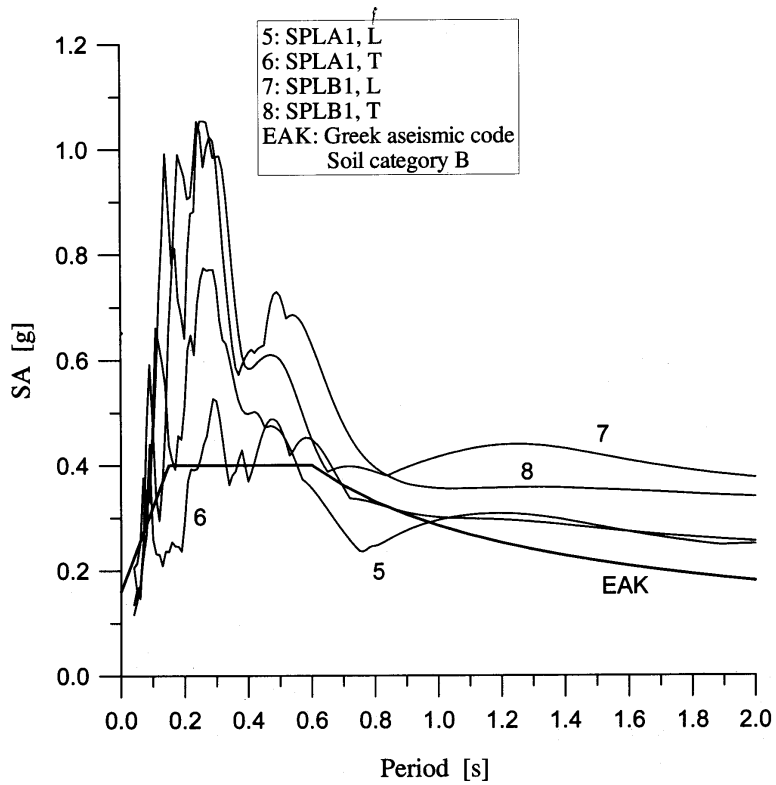

Fig. 3 Elastic response spectra of the accelerograms 5-8 and the recent EAK design spectrum

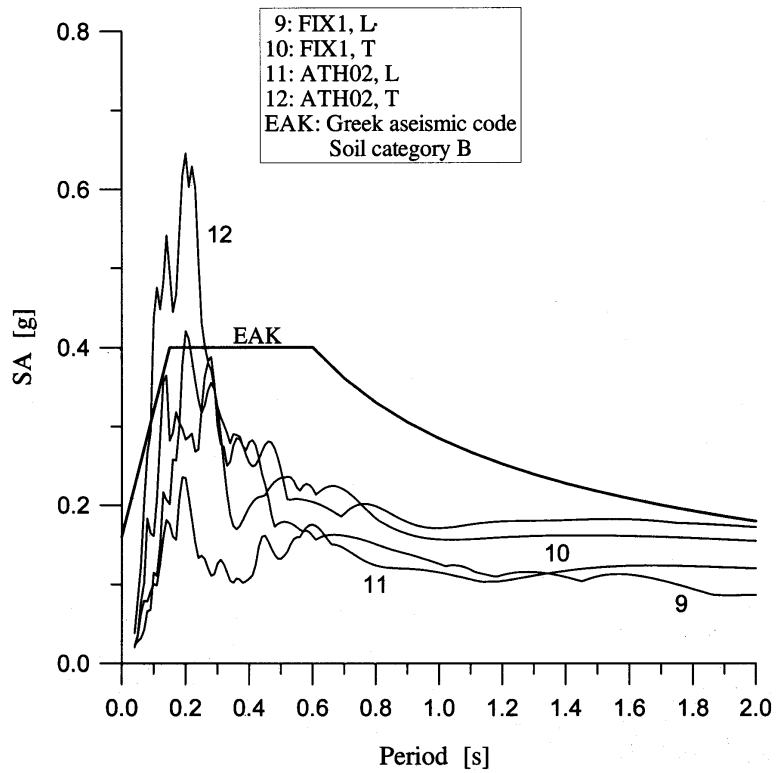

Fig. 4 Elastic response spectra of the accelerograms 9-12 and the recent EAK design spectrum

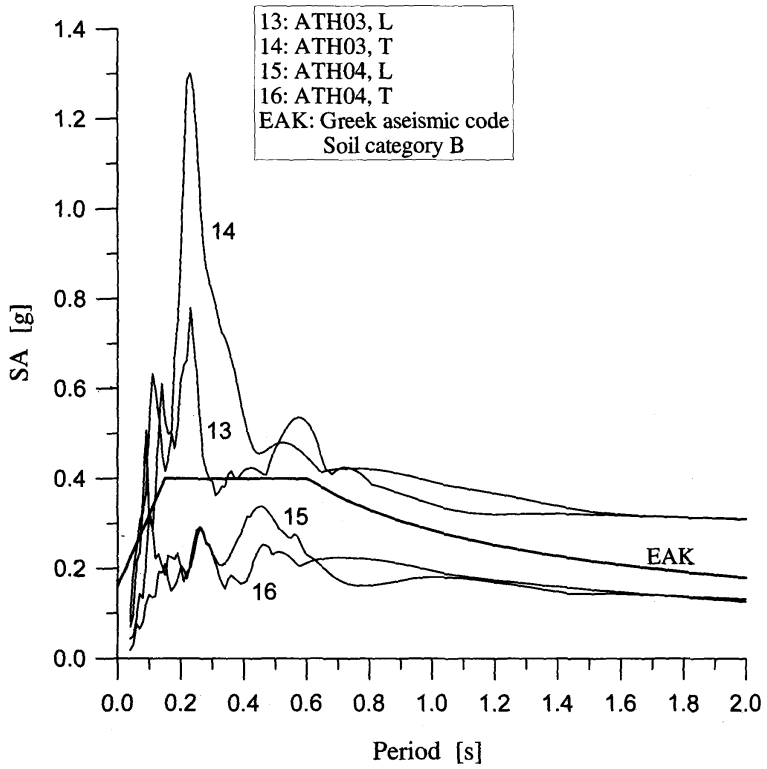

Fig. 5 Elastic response spectra of the accelerograms 13-16 and the recent EAK design spectrum

Table 2: Data of the Used Athens Earthquake Accelerograms

No.	Station	Component	Site Geology	Epicentral Distance (km)
1	Monastiraki (MNSA1)	Longitudinal	Manmade deposits	17
2	Monastiraki (MNSA1)	Transverse	Manmade deposits	17
3	Syntagma A (SGMA1)	Longitudinal	Schist	18
4	Syntagma A (SGMA1)	Transverse	Schist	18
5	Sepolia A (SPLA1)	Longitudinal	Alluvium	15
6	Sepolia A (SPLA1)	Transverse	Alluvium	15
7	Sepolia B (SPLB1)	Longitudinal	Alluvium	15
8	Sepolia B (SPLB1)	Transverse	Alluvium	15
9	Sygrou-Fix (Fix1)	Longitudinal	Alluvium	19
10	Sygrou-Fix (Fix1)	Transverse	Alluvium	19
11	Chalandri (ATH02)	Longitudinal	Alluvium	15
12	Chalandri (ATH02)	Transverse	Alluvium	15
13	Kalithea (ATH03)	Longitudinal	Alluvium	18
14	Kalithea (ATH03)	Transverse	Alluvium	18
15	Kipseli (ATH04)	Longitudinal	Schist	15
16	Kipseli (ATH04)	Transverse	Schist	15

Table 3: Estimated Mean PGA for the Worst Affected Municipalities

Municipality	Mean Distance (km)	Mean PGA (g)
Thrakomakedones	7	0.374
Ano Liosia	3	0.490
Phyli	2	0.530
Nea Philadelphia	12	0.270
Aharnes	4	0.460
Zephyrion	8	0.346
Kamateron	6	0.402
Aspropyrgos	7	0.374
Metamorphosis	8	0.346
Elefsis	12	0.270
Drapetsona	20	0.190
Kifisia	16	0.230

It is well known that seismic parameters exhibit interdependency with observed damages caused by the earthquakes. Therefore, the following seismic parameters are evaluated to describe the severity of the seismic excitation: PGA, $a_{\max}$, ARIAS intensity, I_0, root mean square acceleration, $\mathrm{RMS_a}$, cumulative absolute velocity, CAV, effective peak acceleration, EPA, spectral intensity after Housner, $\mathrm{SI_H}$, spectral intensity after Hidalgo/Clough, $\mathrm{SI_{HC}}$, spectral intensity after Nau/Hall, $\mathrm{SI_{NH}}$, strong motion duration (SMD) after Trifunac/Brady, T_{TB}, the 0.05g bracketed SMD, $T_{0.05}$, power based on SMD after Trifunac/Brady, P_{TB}, and power based on the 0.05g bracketed SMD, $P_{0.05}$.

The ARIAS intensity (Arias, 1970) is a measure of the total energy content of seismic excitation, and is defined by the following relation:

$$I_0 = \frac{\pi}{2\mathrm{g}} \int_0^{t_e} \ddot{x}^2 dt \tag{1}$$

Here, I_0 is the ARIAS intensity, t_e the total seismic duration and $\ddot{x}$ the ground acceleration.

The root mean square acceleration $\mathrm{RMS_a}$ (Meskouris, 2000) is calculated by the following relation:

$$\mathrm{RMS_a} = \sqrt{\frac{1}{t_e} \int_0^{t_e} (\ddot{x})^2 dt} \tag{2}$$

where $\ddot{x}$ is the seismic ground acceleration and t_e the total seismic duration.

The cumulative absolute velocity CAV (Cabanas et al., 1997) is defined as the area under the absolute accelerogram:

$$\mathrm{CAV} = \int_0^{t_e} |\ddot{x}| dt \tag{3}$$

The effective peak acceleration EPA (ATC, 1978; Lungu et al., 1998) is the average of the spectral ordinates of the elastic acceleration response spectrum, $\overline{\mathrm{SA}}$, (for 5% critical damping) in the period interval [0.1 s, 0.5 s], divided by a standard value 2.5. It is defined by the following relation:

$$\mathrm{EPA} = \frac{\overline{\mathrm{SA}}}{2.5} \tag{4}$$

The input seismic energy (Uang and Bertero, 1990) is defined by the following relation:

$$E_{\mathrm{inp}} = m \int_0^{t_e} (\ddot{x} + \ddot{x}_{\mathrm{g}}) \dot{x}_{\mathrm{g}} dt \tag{5}$$

Here, E_{inp} is the input seismic energy of a single degree of freedom (SDOF) system, t_e the total seismic duration, m the mass, x the relative displacement of the system to the ground, and x_g the ground displacement.

According to Housner (Housner, 1952), the definition of spectrum intensity (SI) is given by the relation:

$$\text{SI}_{\text{H}} = \int_{0.1}^{2.5} \text{PSV}(T,\xi)dT \tag{6}$$

where PSV is the pseudo-velocity curve, T is the natural period of a SDOF system, and ξ is the damping coefficient.

Hidalgo and Clough gave a modified definition of SI (Hidalgo and Clough, 1974). They reduced the upper integration limit to 1.0 in comparison to the Housner's definition.

$$\text{SI}_{\text{HC}} = \int_{0.1}^{1.0} \text{PSV}(T,\xi)dT \tag{7}$$

Nau and Hall (1984) defined the spectrum intensity as

$$\text{SI}_{\text{NH}} = \frac{1}{1.715}\int_{0.285}^{2.0} \text{PSV}(T,\xi)dT \tag{8}$$

Because investigations have shown that the seismic energy input response spectra defined by Equation (8) gives a good correlation to damage indices (Elenas, 2000), modified versions of the SI definitions are considered. Those are realised in the above definitions of SI after Housner and after Hidalgo/Clough, by interchanging the pseudo-velocity spectrum with the absolute energy input spectrum. The definition of SI after Nau/Hall is used only in its original form, due to the specific way they defined the integration limits.

The HUSID diagram (Husid, 1969) is used in the definition of the strong motion duration after Trifunac/Brady, and is the time history of the seismic energy content scaled to the total energy content. It is defined by the following relation:

$$H(t) = \frac{\int_0^t (\ddot{x})^2 dt}{\int_0^{t_e} (\ddot{x})^2 dt} \tag{9}$$

$H(t)$ is the HUSID diagram as a function of time t.

The strong motion duration after Trifunac/Brady is defined as time elapsed between 5% and 95% of the HUSID diagram (Trifunac and Brady, 1975), and is defined by the following relation:

$$T_{\text{TB}} = T_{0.95} - T_{0.05} \tag{10}$$

Here, T_{TB} is the strong motion duration, $T_{0.95}$ the time elapsed at the 95% of the HUSID diagram, and $T_{0.05}$ the time elapsed at the 5% of the HUSID diagram.

The "bracketed duration" is the total time elapsed between the first and last excursions of a given level of seismic acceleration. Here, the threshold suggested by Page and co-workers (0.05g) is used (Page et al., 1972).

Finally, power P (Jennings, 1982) is a measure of the energy content per unit time of the seismic excitation, and is defined by the following relation:

$$P = \frac{H_e - H_b}{\text{SMD}} \tag{11}$$

Here, P is the power of the seismic excitation, H_e the energy level at the end of the SMD of the HUSID diagram, H_b the energy level at the beginning of the SMD of the HUSID diagram, and SMD the strong motion duration. In this study, two variants of power definitions are used, corresponding to the two

definitions of SMD: the power based on the SMD after Trifunac/Brady (P_{TB}), and the power based on the 0.05 bracketed SMD $(P_{0.05})$.

Table 4 presents the seismic parameters defined above, for all the seismic records listed in Table 2. Table 5 shows the statistical data of the seismic parameters. As statistical data, the average, the standard deviation, the minimum and maximum values, and the lower and the upper limits of the 95% confidence interval are considered (Spiegel, 1992). The numerical results in Table 5 show that the statistical data from the Athens earthquake records provides great dispersion.

Table 4: Strong Motion Parameters of the Examined Accelerograms

NO.	EVENT	PGA	ARIAS	RMS	CAV	EPA	SI_H		SI_{HC}		SI_{NH}	T_{TB}	$T_{0.05}$	P_{TB}	$P_{0.05}$
		a_{max}	I_0				PSV	E_{inp}	PSV	E_{inp}	PSV				
		(g)	(m/s)	(m/s^2)	(g.s)	(g)	(m)	(m^2/s)	(m)	(m^2/s)	(m/s)	(s)	(s)	(m^2/s^4)	(m^2/s^4)
1	Athens (MNSA1, L)	0.229	0.223	0.228	0.303	0.174	0.503	0.090	0.249	0.061	0.227	5.915	3.695	0.212	0.325
2	Athens (MNSA1, T)	0.511	0.779	0.426	0.471	0.271	0.497	0.086	0.203	0.049	0.193	3.955	5.625	0.829	1.109
3	Athens (SGMA1, L)	0.149	0.095	0.140	0.187	0.115	0.392	0.046	0.154	0.023	0.175	7.095	3.795	0.075	0.130
4	Athens (SGMA1, T)	0.239	0.194	0.201	0.233	0.179	0.380	0.051	0.200	0.034	0.179	3.690	3.815	0.295	0.298
5	Athens (SPLA1, L)	0.245	0.297	0.200	0.316	0.233	0.501	0.080	0.230	0.045	0.235	3.850	2.955	0.433	0.563
6	Athens (SPLA1, T)	0.221	0.178	0.156	0.271	0.159	0.515	0.079	0.206	0.039	0.225	5.110	4.075	0.196	0.245
7	Athens (SPLB1, L)	0.325	0.599	0.285	0.528	0.302	0.617	0.119	0.278	0.068	0.273	5.605	5.480	0.600	0.631
8	Athens (SPLB1, T)	0.312	0.687	0.305	0.555	0.300	0.588	0.131	0.296	0.091	0.263	5.520	6.565	0.699	0.621
9	Athens (Fix1, L)	0.085	0.044	0.095	0.131	0.058	0.367	0.040	0.107	0.010	0.171	5.415	0.885	0.045	0.128
10	Athens (Fix1, T)	0.124	0.068	0.119	0.143	0.100	0.298	0.028	0.132	0.016	0.135	5.245	1.025	0.073	0.288
11	Athens (ATH02, L)	0.110	0.086	0.137	0.192	0.100	0.186	0.017	0.098	0.012	0.086	6.945	2.825	0.070	0.150
12	Athens (ATH02, T)	0.159	0.147	0.180	0.239	0.121	0.296	0.032	0.096	0.011	0.126	7.110	2.925	0.117	0.267
13	Athens (ATH03, L)	0.264	0.331	0.230	0.370	0.189	0.521	0.098	0.291	0.078	0.241	5.850	11.525	0.318	0.174
14	Athens (ATH03, T)	0.303	0.434	0.263	0.381	0.246	0.503	0.084	0.232	0.053	0.211	4.370	5.310	0.559	0.487
15	Athens (ATH04, L)	0.121	0.094	0.146	0.188	0.107	0.273	0.031	0.151	0.022	0.133	6.510	2.585	0.081	0.181
16	Athens(ATH04, T)	0.110	0.065	0.122	0.158	0.084	0.372	0.043	0.131	0.016	0.164	5.020	2.875	0.073	0.113

Table 5: Statistical Data of the Seismic Parameters of the Athens Accelerogram Records

Seismic Parameters		Average	Standard Deviation	Minimum Value	Maximum Value	95% Confidence Interval for Mean	
						Lower Limit	Upper Limit
PGA (g)		0.219	0.11	0.085	0.511	0.16	0.278
ARIAS (m^2/s^3)		0.27	0.235	0.044	0.779	0.144	0.395
RMS (m/s^2)		0.202	0.086	0.095	0.426	0.156	0.248
CAV (g.s)		0.291	0.135	0.131	0.555	0.219	0.363
EPA (g)		0.171	0.079	0.058	0.302	0.129	0.213
SI_H	PSV (m)	0.425	0.122	0.186	0.617	0.36	0.491
	E_{inp} (m^2/s)	0.066	0.034	0.017	0.131	0.047	0.084
SI_{HC}	PSV (m)	0.191	0.068	0.096	0.296	0.154	0.227
	E_{inp} (m^2/s)	0.039	0.025	0.01	0.091	0.025	0.053
SI_{NH} (m/s)		0.19	0.053	0.086	0.273	0.161	0.218
T_{TB} (s)		5.45	1.114	3.69	7.11	4.856	6.044
$T_{0.05}$ (s)		4.122	2.518	0.885	11.525	2.781	5.465
P_{TB} (m^2/s^4)		0.292	0.256	0.045	0.829	0.155	0.428
$P_{0.05}$ (m^2/s^4)		0.357	0.267	0.113	1.109	0.214	0.499

Figures 2 to 5 show the elastic acceleration response spectra (5% damping) of all accelerograms included in Table 2, and the elastic design spectrum for the soil category B (medium soil) of the recent Greek aseismic code (EAK-2000). These figures expose the variations in spectral values, although the epicentral distances are comparable for all the examined records. This fact points to the evidence of the influence of the local conditions on the strong ground motion. It can be observed that the numerical values of the response spectra of several records are greater than the values of the design spectra, especially in the low period range.

DAMAGES TO BUILDINGS

The day following the earthquake event, the Ministry of Environment, Urban Planning and Public Works organized numerous two-person teams of engineers, which began surveying the affected areas for a rapid damage assessment. Most of the damages after the earthquake were observed within a distance of 12 km of the epicentre. Structural damages were found rapidly to decrease with the distance from the epicentre. In most areas of Athens, damage was non-structural (e.g., cracks in infill brick walls). The distribution of damage intensity showed anisomorphism, which was identified to be due to the geological site conditions. Additionally, poor foundation conditions (e.g., artificial fill) or the local topography played a dominant role.

Table 6 summarises the housing damage statistics for the 12 worst affected municipalities (ESYE, 2000). The last column shows the Modified Mercalli Intensity (MMI) experienced within each municipality (Pomonis, 2002). The population and the total number of dwelling units were obtained from the last available Greek census (carried out in April, 1991 and December, 1990, respectively). The damage ratio (DR) is the quotient of red and yellow dwelling units over their estimated total number at the time of the earthquake. The bottom row of Table 6 presents damage statistics for the sum of the remaining 30 municipalities in the capital region. These municipalities are mainly in the intensity VI zone, and were lightly affected. In addition, Table 6 shows that the damage ratio of the 5 municipalities closest to the epicentre (Phyli, Ano Liosia, Aharnes, Thracomakedones, and Nea Philadelphia) was more than 40%.

Table 6: Housing Damage Statistics

Municipality	Population	Dwelling Units	Red	Yellow	Red + Yellow	Approximate DR	MMI
Thracomakedones	3135	1204	82	923	1005	84%	VII–VIII
Ano Liosia	21397	6844	1107	3132	4239	62%	VI–IX
Phyli	2925	909	135	374	509	56%	VII–IX
Nea Philadelphia	25261	10155	399	3766	4165	41%	VI–VIII
Aharnes	59698	20504	1340	7200	8540	42%	VII–IX
Zephyrion	8985	2378	61	858	919	39%	VI–VII
Kamateron	17410	6506	140	1410	1550	24%	VI–VIII
Aspropyrgos	15034	5651	175	881	1056	19%	VI–VII
Metamorphosis	21052	7691	115	1481	1596	21%	VI–IX
Elefsis	22793	7960	105	1065	1170	15%	VI–VII
Drapetsona	13094	5116	154	611	765	15%	VI
Kifisia	39166	15535	168	1283	1451	9%	VI–VII
Total	249950	90453	3981	22984	26965	30%	VI–IX
Remaining 30 Municipalities	2848825	958716	1835	42692	44527	5%	V–VII

Table 7 gives the statistical data of building properties in the municipality of Ano Liosia, which, as shown in Table 6, has the maximum DR (62%) in the meizoseismal area (MMI equal to IX). In detail, Table 7 presents the percentage of the buildings according to the number of storeys, the year of construction, and the type of load-bearing system. The year of construction is related with the dates of major revisions in the national aseismic design code provisions. In 1959, the aseismic design code of Greece was introduced, and it has been revised in 1984 and 1995. The building properties were almost uniformly distributed. In contrast, the damages were concentrated in the central and southern regions, which can be attributed to the effect of the local soil conditions. Nevertheless, reinforced concrete

structures showed enhanced seismic resistance than masonry buildings. In addition, the vulnerability of buildings built after 1984, and furthermore after 1995, was significantly reduced.

Table 7: Statistical Data of Building Properties in the Municipality of Ano Liosia

		Percentage of Buildings
Number of Storeys	**1**	52
	2	38
	3	8
	>4	2
Date of Construction	**Before 1959**	6
	Between 1959-1985	67
	Between 1986-1995	20
	After 1995	7
Type of Structure	**Masonry**	62
	Masonry and R/C	14
	R/C	13
	Others	11

While focussing on the twelve worst affected municipalities, correlation coefficients have been used to emphasise the grade of interrelation among the approximate damage ratios, the MMI values, the mean distance from the seismic epicentre, and the PGA. The numerical values of these quantities have been given in Tables 3 and 6. It is assumed that a correlation coefficient up to 0.5 means low correlation, a coefficient in the range, 0.5-0.8, means medium correlation, while a coefficient greater than 0.8 means strong correlation. Table 8 shows the Pearson correlation matrix, while Table 9 shows the Spearman rank correlation matrix among the examined data. The correlation coefficient after Pearson shows how well the data follows a linear relationship, whereas the coefficient after Spearman shows how well the data follows a monotonic ranking (Spiegel, 1992). The correlation matrices are symmetric, and quantities that furnish a coefficient greater than 0.602, exhibit significant correlation at the 0.1% level (2-tailed).

Through the Pearson correlation coefficient, numerically shown in Table 8, it can be seen that the damage ratios have a medium correlation with the minimum, maximum and mean values of MMI, the mean distance, and the PGA. Furthermore, the mean distance has medium and negative correlation with all other quantities. The best negative correlation is observed between PGA and mean distance (-0.966), while the best positive correlation is obtained between mean and maximum MMI (0.954), and between PGA and mean MMI (0.818).

Table 8: Pearson Correlation Matrix

	Pearson Correlation Coefficients					
	Approximate DR	**Min MMI**	**Max MMI**	**Mean MMI**	**Mean Distance**	**PGA**
Approximate DR	1.000	0.663	0.543	0.655	-0.602	0.610
Min MMI	0.663	1.000	0.488	0.728	-0.497	0.793
Max MMI	0.543	0.488	1.000	0.954	-0.798	0.793
Mean MMI	0.655	0.728	0.954	1.000	-0.798	0.818
Mean Distance	-0.602	-0.497	-0.798	-0.798	1.000	-0.966
PGA	0.610	0.564	0.793	0.818	-0.966	1.000

Table 9: Spearman Rank Correlation Matrix

	Spearman Rank Correlation Coefficients					
	Approximate DR	**Min MMI**	**Max MMI**	**Mean MMI**	**Mean Distance**	**PGA**
Approximate DR	1.000	0.642	0.701	0.777	-0.741	0.741
Min MMI	0.642	1.000	0.495	0.717	-0.560	0.560
Max MMI	0.701	0.495	1.000	0.959	-0.757	0.757
Mean MMI	0.777	0.717	0.959	1.000	-0.789	0.789
Mean Distance	-0.741	-0.560	-0.757	-0.789	1.000	-1.000
PGA	0.741	0.560	0.757	0.789	-1.000	1.000

Table 9 shows the Spearman rank correlation matrix. These results coincide with the Pearson correlation matrix. Thus, the damage ratios have medium correlation with the other quantities. Furthermore, the DR, the MMI values, and the PGA decrease with increasing mean distance from the seismic epicentre, as is manifested by the negative rank correlation coefficients. The best correlation is observed between PGA and mean distance (-1.0). This explains the coincidence of the absolute values, and the opposite signs, of the correlation coefficients of mean distance and PGA with the other quantities.

In the larger area of Athens, several reinforced concrete buildings sustained severe structural damage, and some of them collapsed, either totally or partially. Most of the severely damaged structures were designed according to the older seismic codes (of 1959 or 1984), with lower seismic forces than those experienced during the earthquake. In addition, these buildings provided low ductility capacity. Typically, the damaged buildings in the meizoseismal area were two-storey to five-storey. Often, their concrete and construction quality was poor.

The most widely observed damages to reinforced concrete frame buildings can be classified according to the cause of damage, as follows:

1. Damage to column-beam joints due to bad concrete quality and insufficient reinforcement. Often, stirrup reinforcement was almost non-existent.
2. Shear failure damage to columns due to the short column effect, with rapid decrease of vertical load-bearing capacity.
3. Damage to buildings with a soft ground floor. Buildings with a soft ground floor are a common practice in Greece. Much less rigidity in this floor, compared with the rest of the building, leads to large deformations of the soft storey. The damage occurred mainly to the joints, which were destroyed in most of the cases.

Moreover, during the post-earthquake inspection process, corrosion problems were observed, which during the earthquake resulted in the splitting of the cover concrete, and were caused by the lack of structural maintenance.

Numerical analyses have been performed for the simulation of the behaviour of several damaged (Elenas et al., 2002; Decanini et al., 2002) or collapsed (Kiousis and Karabinis, 2002) buildings. The results correlated well with the observed damages, and confirmed the main causes of the damages (soft storeys, poor material quality, and insufficient reinforcement).

Significant damages were observed in the masonry structures in the meizoseismal area. Most adobe houses and stone masonry structures with undressed stones, constructed in the first half of the century, suffered considerable damages. This included partial collapse of external walls, collapses of corners, separation of the two walls converging at a corner, and extensive cracking. On the other hand, brick masonry houses with reinforced concrete lintel bands or concrete roof slabs, built in recent years, survived with less damage.

No major damage was reported to bridges. No damages were reported to the underground metro of Athens and to the recently built natural gas network, although pipelines of high pressure were crossing the meizoseismal area at a depth of approximately 1.5 m. No damage was reported to the road or rail network, excepting a road (leading to the summit of Mount Parnitha), which was very close to the epicentre. In many locations, the roads were constructed partly on excavation and partly on fills. Severe landslides in these fills caused collapse of the masonry barrier of the road. In addition, large pieces of rocks slid into the pavement. In regions close to the epicentre, minor leakages were observed in service connections and some larger pipelines (diameter of 1100, 1700 and 1800 mm) of the water supply network. The wastewater network did not suffer any considerable damage.

From an economic point of view, harbours are important facilities for a region. The harbours of Piraeus and Elefsis are at epicentral distances greater than 15 km. There, reported damages were generally minor. Some gravity quay walls settled and moved outwards by about 10 cm. In the latter case, this deformation caused distortion of crane rails and damages to electric power lines. No damages were reported to piers on pile foundations.

Fig. 6 Exposed column reinforcement bar without stirrups

Fig. 7 Exposed anchorage hook without stirrups at a column

Figure 6 shows insufficient stirrups at the bottom of a column, at the soft ground floor of a 10-storey reinforced concrete building. Stirrups are absent up to a height of 1.20 m. Figure 7 presents an exposed reinforcement anchorage hook without stirrups at the base of a column. Figure 8 shows a buckled longitudinal reinforcement bar of a column. All these figures underline the absence of stirrups in critical regions.

Fig. 8 Buckled reinforcement bar and minimal stirrups

Figure 9 shows damages at the top of columns due to inadequate reinforcement. The columns were placed in the soft ground floor of a reinforced concrete building. Soft storeys frequently led to minor or heavy damages, up to the point of collapse. Figure 10 shows column damage in a soft storey, and the reinforcement deficiency is obvious. An x-shaped crack on a reinforced concrete wall is presented in Figure 11. It is placed at the soft ground floor of a building. A very common observed failure is the x-

shaped crack in short columns, as shown in Figure 12. In addition, Figure 13 presents a shear crack in a short column due to insufficient confinement. Figure 14 shows the partial collapse of a staircase, due to short anchorage length of the longitudinal reinforcement. The mid-part building collapse presented in Figure 15 was caused by short anchorage length of the longitudinal reinforcement of the mid-part beam. Figure 16 shows the partial collapse of a building, initiated by the failure of a column at the soft ground floor.

Fig. 9 Damaged beam-column joint in a soft first storey

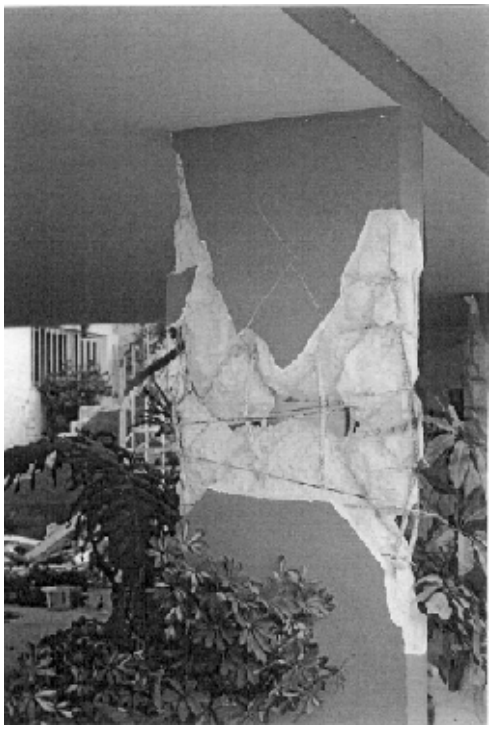

Fig. 10 Failure of column in a soft first storey

Fig. 11 X-shaped shear crack on a reinforced concrete wall

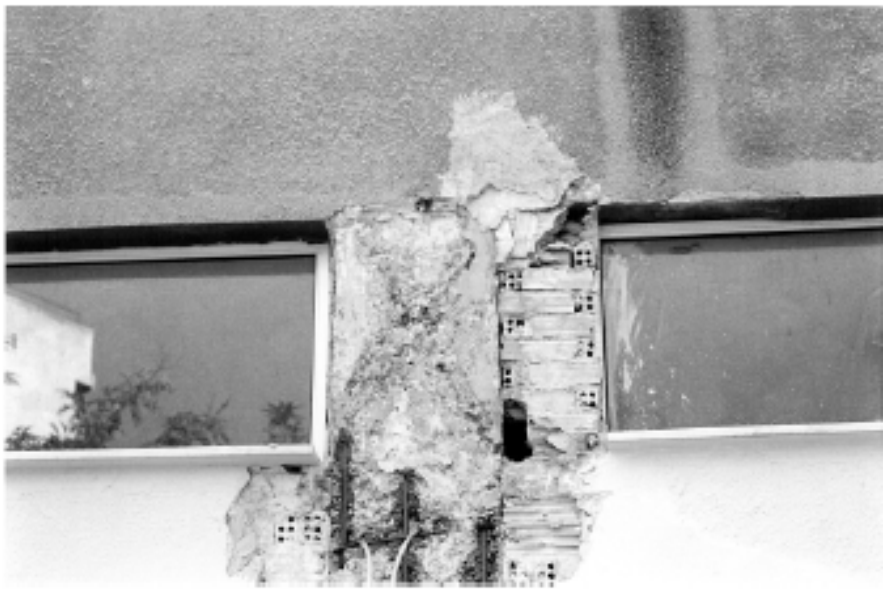

Fig. 12 X-shaped crack in a short column

Unexpected installations put into structural components led to damages. For example, Figure 17 shows a drainage pipe built into a collapsed column. Poor stirrup reinforcement can also be observed. Moreover, Figure 18 shows an electrical cable installation built at the top of a column, which decreases the column strength in a potential plastic hinge region. Figure 19 shows hooks of longitudinal wall reinforcement of a 10-storey reinforced concrete structure, terminated just above the floor slab. It is obviously an inadequate anchorage of wall-reinforcement. In the same building, large gaps due to improper concrete pouring and compacting were observed, as shown in Figure 20.

Fig. 13 Shear crack in a short column

Fig. 14 Partial collapses of a staircase

Fig. 15 Collapse of the middle part of a building

Fig. 16 Partial collapse of a reinforced concrete building

Fig. 17 Pipe for drainage put into a column

Fig. 18 Electrical cable installation put in a column

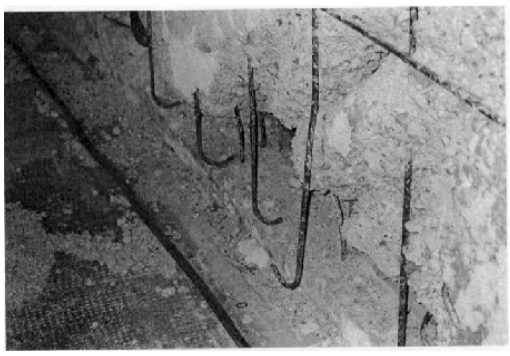

Fig. 19 Inadequate anchorage of a wall-reinforcement

Fig. 20 Large gaps due to improper concrete pouring and compacting

Pounding effects among adjacent structural elements or buildings led frequently to damages. For example, Figure 21 shows damage caused by pounding between a stone masonry and a reinforced concrete structure. In addition, a beam failure caused by pounding between the beam and the column next to it, is shown in Figure 22. It points to shear failure in a short beam. Furthermore, deficiencies in the construction of gaps also led to damages, as is shown in Figure 23. Here, a reinforced concrete column and wall are separated by an improper expansion gap. In addition, Figure 24 exposes a simulated expansion gap. Here, the columns were initially built together. After that, an electrical cutting machine has cut a 5 cm deep gap. During this process, the stirrups have also been cut. Moreover, the gap was filled with polystyrol material to simulate a properly constructed gap. Frequently observed damages were x-shaped cracks in masonry infill walls, as shown in Figure 25. Figure 26 shows a collapsed roof parapet, lying at the playground of the school.

Fig. 21 Damage due to pounding of adjacent building

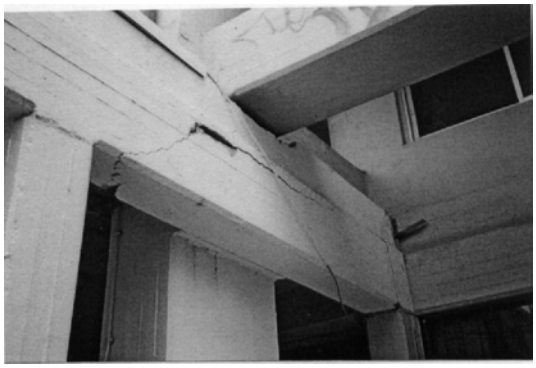

Fig. 22 Failure of a beam due to pounding

Fig. 23 Improper construction of a gap

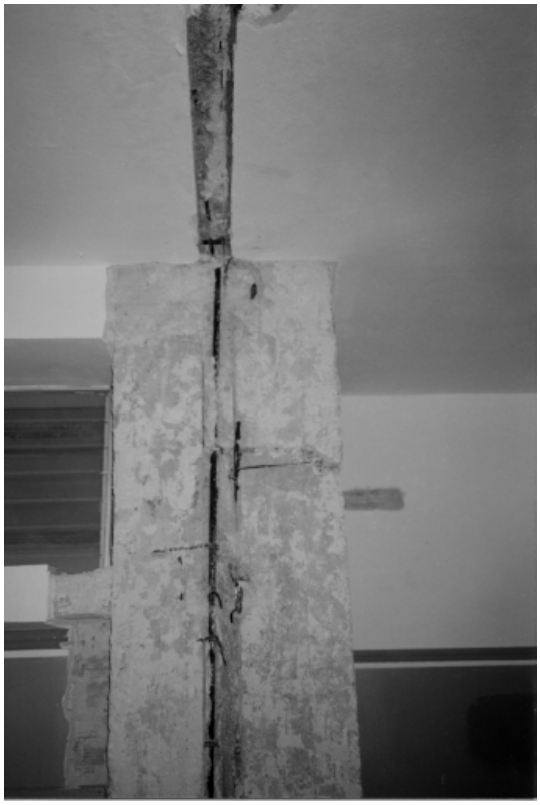

Fig. 24 Damage in a simulated expansion gap

Fig. 25 Masonry failure with x-shaped cracks

Fig. 26 Collapse of a roof parapet

During the post-earthquake inspection process, several deficiencies were observed in the architectural design of buildings. As examples are presented first, a weak column and strong beam system, as shown in Figure 27. Plastic hinges may appear at the columns, which is an undesirable phenomenon during seismic excitation. Secondly, a long cantilever beam system (up to ten metres) is used for sun protection, as shown in Figure 28. In the latter case, additional mass is added to the dynamical system of the building. Furthermore, because it was built at the beginning of 1960's, there is a reason to believe that no special design considerations were made to resist seismic vertical vibrations. Although no significant damages were found on those buildings, the architectural deficiencies can be protagonists in a future earthquake.

Fig. 27 A weak column and strong beam system

Fig. 28 A long cantilever beam system

CONCLUSIONS

The numerical analysis of the accelerograms recorded during the 1999 Athens earthquake has shown that the seismic parameters of the Athens earthquake exhibit a great dispersion in the results. Both low and high numerical values have been observed for all the examined engineering parameters, due to the different geological conditions (e.g., the PGA varied from 0.085g to 0.511g). The destructive

consequences may be attributed first to the proximity of the epicentre to the urban area, and secondly to the high vulnerability of several structures.

Correlation coefficients have been calculated to expose the grade of interrelation among the damage ratios, the MMI values, the mean distance from the seismic epicenter, and the PGA, for the twelve worst affected municipalities. The damage ratios show medium correlation with the other quantities. Furthermore, the damage ratios, the MMI values, and the PGA decrease with increasing mean distance from the seismic epicentre, as is manifested by the negative correlation coefficients. The best correlation is observed between PGA and mean distance (-0.966 Pearson correlation and -1.0 Spearman rank correlation). The correlation matrices after Pearson and after Spearman, point to the same interrelation grade among the investigated quantities.

Bad concrete quality and insufficient reinforcement led to damages to column-beam joints. Additional reasons of observed damages were: insufficient anchorage lengths, short column effects, and absence of infill walls in soft ground floors. The same reasons led to a deficiency in member and structural ductility.

Most of the structural damages were attributed mainly to poor structural detailing and inappropriate construction, than to wrong structural analysis. Therefore, the use of more conservative seismic design coefficients alone cannot ensure the safety of structures, unless this is part of proper seismic design criteria and provisions, including structural detailing and construction. To avoid considerable damages during the seismic excitations of medium severity, efforts must be made for the upgradation of existing buildings so as to ensure the security level of recent seismic codes, if this is economically feasible.

ACKNOWLEDGMENTS

The disposition of the acceleration records from the Institute of Geodynamics of the National Observatory of Athens, Greece and from the Institute of Engineering Seismology and Earthquake Engineering (ITSAK), Thessaloniki, Greece, is gratefully acknowledged.

REFERENCES

1. Anastasiadis, A., Demosthenous, M., Karakostas, C., Klimis, N., Lekidis, B., Margaris, B., Papaioannou, C., Papazachos, C. and Theodulidis, N. (1999). “The Athens (Greece) Earthquake of September 7, 1999: Preliminary Report on Strong Motion Data and Structural response”, Institute of Engineering Seismology and Earthquake Engineering (ITSAK), Thessaloniki, Greece.
2. Arias, A. (1970). “A Measure of Earthquake Intensity”, in “Seismic Design for Nuclear Power Plants (edited by R. Hansen)”, MIT Press, Cambridge (MA), U.S.A., pp. 438-469.
3. ATC (1978). “Tentative Provisions for the Development of Seismic Regulations for Buildings”, ATC 3-06, Applied Technology Council, U.S.A.
4. Bouckovalas, G.D. and Kouretzis, G.P. (2001). “Stiff Soil Amplification Effects in the 7 September 1999 Athens (Greece) Earthquake”, Soil Dynamics and Earthquake Engineering, Vol. 21, No. 8, pp. 671-687.
5. Bouckovalas, G.D., Kouretzis, G.P. and Kalogeras, I.S. (2002). “Site Specific Analysis of Strong Motion Data from the September 7, 1999 Athens, Greece Earthquake”, Natural Hazards, Vol. 27, No. 2, pp. 105-131.
6. Cabanas, L., Benito, B. and Herraiz, M. (1997). “An Approach to the Measurement of the Potential Structural Damage of Earthquake Ground Motions”, Earthquake Engineering and Structural Dynamics, Vol. 26, No. 1, pp. 79-92.
7. Decanini, L., De Sortis, A., Liberatore, L. and Mollaioli, T. (2002). “Damage Characterisation of the 1999 Athens Earthquake”, CD-ROM Proceedings of the 12th European Conference on Earthquake Engineering, Elsevier, Amsterdam, The Netherlands, Paper 287.
8. Elenas, A. (2000). “Correlation between Seismic Acceleration Parameters and the Overall Damage Indices of Buildings”, Soil Dynamics and Earthquake Engineering, Vol. 20, No. 1, pp. 93-100.
9. Elenas, A., Vasiliadis, L. and Dimova, S. (2002). “Numerical Estimation of the Dynamical Response of a Seismic Retrofitted Reinforced Concrete Building”, Proceedings of the 5th European Conference on Structural Dynamics (EURODYN 2002), Balkema, Lisse, The Netherlands, pp. 1353-1358.

10. ESYE (2000). "Summary Tables of Damage by Municipality for Households and Businesses", National Statistical Service of Greece, Athens, Greece.
11. Gazetas, G., Kallou, P.V. and Psarropoulos, P.N. (2002). "Topography and Soil Effects in the M_S 5.9 Parnitha (Athens) Earthquake: The Case of Adames", Natural Hazards, Vol. 27, No. 2, pp. 133-169.
12. Hidalgo, P. and Clough, R.W. (1974). "Earthquake Simulator Study of a Reinforced Concrete Frame", Report UCB/EERC-74/13, EERC, University of California, Berkeley, U.S.A.
13. Housner, G.W. (1952). "Spectrum Intensities of Strong Motion Earthquakes", Proceedings of Symposium on Earthquake and Blast Effects on Structures, EERI, Oakland, California, U.S.A., pp. 20-36.
14. Husid, R.L. (1969). "Analisis de Terremoros: Analisis General", Revista del IDIEM, Vol. 8, No. 1, pp. 21-42.
15. Jennings, P.C. (1982). "Engineering Seismology", in "Earthquakes: Observation, Theory and Interpretation (edited by H. Kanamori and E. Boschi)", Italian Physical Society, Varenna, Italy, pp. 138-173.
16. Kalogeras, I.S. and Stavrakakis, G.N. (1999). "Processing of the Strong Motion Data from the September 7th, 1999 Athens Earthquake", Publication No. 10, Institute of Geodynamics of the National Observatory, Athens, Greece.
17. Kiousis, P.D. and Karabinis, A.I. (2002). "Investigation of Collapse Mechanism of an Apartment Building during the Earthquake of Athens on 7-9-1999", CD-ROM Proceedings of the 12th European Conference on Earthquake Engineering, Elsevier, Amsterdam, The Netherlands, Paper 555.
18. Lekkas, E. (2001). "The Athens Earthquake (7 September 1999): Intensity Distribution and Controlling Factors", Engineering Geology, Vol. 59, No. 4, pp. 297-311.
19. Lungu, D., Aldea, A., Zaicenco, A. and Cornea, T. (1998). "PSHA and GIS Technology - Tools for Seismic Hazard Macrozonation in Eastern Europe", CD-ROM Proceedings of the 11th European Conference on Earthquake Engineering, Balkema, Rotterdam, The Netherlands.
20. Meskouris, K. (2000). "Structural Dynamics", Ernst & Sohn, Berlin, Germany.
21. Nau, M. and Hall, W.J. (1984). "Scaling Methods for Earthquake Response Spectra", Journal of Structural Engineering, Vol. 110, No. 7, pp. 1533-1548.
22. Page, R.A., Boore, D.M., Joyner, W.B. and Coulter, H.W. (1972). "Ground Motion Values for Use in Seismic Design of Trans-Alaska Pipeline System", USGS Circular 672, U.S. Geological Survey, Washington, D.C., U.S.A.
23. Papadopoulos, G.A., Drakatos, G., Papanastassiou, D., Kalogeras, I. and Stavrakakis, G. (2000). "Preliminary Results about the Catastrophic Earthquake of 7 September 1999 in Athens, Greece", Seismological Research Letters, Vol. 71, No. 3, pp. 318-329.
24. Pomonis, A. (2002). "The Mount Parnitha (Athens) Earthquake of September 7, 1999: A Disaster Management Perspective", Natural Hazards, Vol. 27, No 2, pp. 171-199.
25. Psycharis, I., Papastamatiou, I., Taflambas, I., Carydis, P., Bouckovalas, G., Gazetas, G., Kalogeras, I., Stavrakakis, G., Pavlides, S., Lekkas, E., Kranis, C., Ioannidis, C., Cholevas, C. and Pyrros, D. (1999). "The Athens, Greece Earthquake of September 7, 1999", Special Earthquake Report, EERI Newsletter, Vol. 33, No. 11, pp. 1-12.
26. Spiegel, M.R. (1992). "Theory and Problems of Statistics", McGraw-Hill, London, U.K.
27. Trifunac, M.D. and Brady, A.G. (1975). "A Study on the Duration of Strong Earthquake Ground Motion", Bulletin of the Seismological Society of America, Vol. 65, No. 3, pp. 581-626.
28. Tselentis, G.A. and Zahradnik, J. (2000). "The Athens Earthquake of 7 September 1999", Bulletin of the Seismological Society of America, Vol. 90, No. 5, pp. 1143-1160.
29. Uang, C.-M. and Bertero, V.V. (1990). "Evaluation of Seismic Energy in Structures", Earthquake Engineering and Structural Dynamics", Vol. 19, No. 1, pp. 77-90.